Connexin 47 (Cx47)-Deficient Mice with Enhanced Green Fluorescent Protein Reporter Gene Reveal Predominant Oligodendrocytic Expression of Cx47 and Display Vacuolized Myelin in the CNS

Benjamin Odermatt,[1] Kerstin Wellershaus,[1] Anke Wallraff,[3] Gerald Seifert,[3] Joachim Degen,[1] Carsten Euwens,[1] Babette Fuss,[4] Heinrich Büssow,[2] Karl Schilling,[2] Christian Steinhäuser,[3] and Klaus Willecke[1]

[1]Institut für Genetik, Universität Bonn, D-53117 Bonn, Germany, [2]Anatomisches Institut, Universität Bonn, D-53115 Bonn, Germany, [3]Experimentelle Neurobiologie, Neurochirurgie, Universität Bonn, D-53105 Bonn, Germany, and [4]Department of Anatomy and Neurobiology, Virginia Commonwealth University, Richmond, Virginia 23298

To further characterize the recently described gap junction gene connexin 47 (Cx47), we generated Cx47-null mice by replacing the Cx47 coding DNA with an enhanced green fluorescent protein (EGFP) reporter gene, which was thus placed under control of the endogenous Cx47 promoter. Homozygous mutant mice were fertile and showed no obvious morphological or behavioral abnormalities. Colocalization of EGFP fluorescence and immunofluorescence of cell marker proteins revealed that Cx47 was mainly expressed in oligodendrocytes in highly myelinated CNS tissues and in few calcium-binding protein S100 β subunit-positive cells but not in neurons or peripheral sciatic nerve. This corrects our previous conclusion that Cx47 mRNA is expressed in brain and spinal cord neurons (Teubner et al., 2001). Cx47 protein was detected by Western blot analysis after immunoprecipitation in CNS tissues of wild-type mice but not in heart or Cx47-deficient tissues. Electron microscopic analysis of CNS white matter in Cx47-deficient mice revealed a conspicuous vacuolation of nerve fibers, particularly at the site of the optic nerve where axons are first contacted by oligodendrocytes and myelination starts. Initial analyses of Cx32/Cx47-double-deficient mice showed that these mice developed an action tremor and died on average at 51 d after birth. The central white matter of these double-deficient mice exhibited much more abundant vacuolation in nerve fibers than mice deficient only in Cx47.

Key words: **EGFP; gap junctions; oligodendrocytes; glia cells; vacuolation; Cx32/Cx47 double-deficient mice**

Introduction

Connexins are protein subunits of hexameric hemichannels (connexons) in the plasma membrane of vertebrate cells. Hemichannels in contacting cells can dock to each other, thus forming intercellular conduits or gap junction channels, which provide electrotonic and metabolic communication. Twenty human and 19 mouse connexin genes have been identified (White and Paul, 1999; Eiberger et al., 2001; Willecke et al., 2002). Increasing morphological and physiological evidence indicates that gap junctional intercellular communication in the mammalian CNS is a common phenomenon (Rash et al., 2001a; Traub et al., 2002). Recently we reported the cloning and initial characterization of the mouse connexin 47 gene (Cx47) (Teubner et al., 2001), whose mRNA, based on *in situ* hybridization analysis, was localized to CNS neurons. This conclusion, however, has recently been challenged by Menichella et al. (2001), who reported in an abstract that Cx47 mRNA is expressed by oligodendrocytes.

Disruption of connexin genes has led to novel insights into the biological function of gap junctions (Simon and Goodenough, 1998; Lo, 1999; Willecke et al., 2002). Here we describe the generation of Cx47-deficient mice in which the Cx47 coding region was replaced by cDNA coding for the enhanced variant of the green fluorescent protein (EGFP) (Chalfie et al., 1994; Cubitt et al., 1995), which, consequently, was placed under control of the Cx47 promoter (for nomenclature of mouse genotype, see Materials and Methods). In these animals, EGFP fluorescence should allow unequivocal identification of specific cell types expressing Cx47 mRNA. Moreover, it should ease recognition and patch-clamp recording of Cx47-expressing cells in acute tissue slices.

We find that Cx47-deficient mice are fertile and show no obvious gross anatomical or behavioral abnormalities. A combined immunocytochemical, physiological, and ultrastructural analysis of these animals revealed that Cx47 is expressed in oligodendrocytes and some calcium-binding protein S100 β subunit (S100β)-positive cells, i.e., presumed astrocytes. Thus, they did not confirm our previous conclusion (Teubner et al., 2001) that Cx47 mRNA is expressed in neurons. Presumably, our probe used for *in situ* hybridization cross-reacted with an unknown transcript in neurons. Electron microscopic investigation of the

Received Jan. 2, 2003; revised March 20, 2003; accepted March 21, 2003.

This work was supported by German Research Association Grants JA 942/4-1, SFBs 400, and TR3 and Fonds of the Chemical Industry (C.S. and K.W.). B.O. received a stipend from the Graduiertenkolleg Pathogenese des Nervensystems. We gratefully acknowledge the excellent technical assistance of Ina Fibich, Joana Fischer, Michaela Lindemann, Ingrid Krahner, and Gaby Schwarz and thank Dr. Alberto Perez-Bouza for suggestions and comments on this work.

Correspondence should be addressed to Dr. Klaus Willecke, Institut für Genetik, Universität Bonn, Römerstrasse 164, D-53117 Bonn, Germany. E-mail: genetik@uni-bonn.de.

 0270-6474/03/234549-11$15.00/0

optic nerve and other CNS tissues in Cx47$^{EGFP(-/-)}$ mice revealed abnormal myelin vacuolation of nerve fibers.

To corroborate the significance of Cx47 for myelination (Scherer and Chance, 1995) and oligodendrocyte function, we also analyzed mice deficient for both Cx47 and Cx32. This latter connexin is known to be expressed in oligodendrocytes (Li et al., 1997; Scherer et al., 1998). Cx32/Cx47-double-deficient mice died on average after 51 d and displayed delayed myelination and a much stronger vacuolation of CNS nerve fibers than mice with Cx47 deficiency only. Myelination of peripheral nerves did not seem to be affected in Cx47- or Cx32/Cx47-deficient mice.

Materials and Methods

Construction of the targeting Cx47^{EGFP} vector

The targeting construct consisted of two arms of homologous genomic DNA flanking the Cx47 coding region: a 5′ 2.0 kb *Kpn*I–*Aci*I fragment and a 3′ 5.5 kb *Eco*RI–*Eco*RV fragment separated by a 1 kb *Nco*I–*Afl*II EGFP-SV40 poly(A) fragment from pEGFP-1 (Clontech; Palo Alto, CA) with deleted *Not*I and *Xba*I sites. The ATG translational start codon of the EGFP gene was inserted blunt-ended in-frame after the first seven codons of Cx47. A hypoxanthine phosphoribosyltransferase (HPRT) minigene driven by the mouse phosphoglycerate kinase (PGK) promoter (Magin et al., 1992), in the opposite direction from Cx47 and EGFP, was additionally cloned in front of the 3′ homologous flanking region. The EGFP coding DNA and the HPRT minigene replaced the remaining coding region of Cx47 and 560 bp of the 3′ untranslated region (Fig. 1*a*). The final targeting vector was restriction-mapped, and the Cx47-EGFP transition region was sequenced. The DNA (250 μg) of the targeting vector was linearized by *Not*I digestion and transfected by electroporation into HPRT-deficient and feeder-independent HPRT Minus (HM-1) embryonic stem (ES) cells (Magin et al., 1992, 1998). Cell culture and selection of targeted colonies using hypoxanthine-aminopterine-thymidine (HAT) medium were performed according to standard protocols (Selfridge et al., 1992; Theis et al., 2000).

Screening of ES cell clones

Homologous recombination in HAT-resistant ES cell clones was screened using PCR and subsequently confirmed by Southern blot hybridization.

Hot start PCR screening for homologous recombined cell clones was performed using a 5′ sense primer (P2; 5′-CTGAGAGTGGACAGGTCCCTTTGAAGG) external to the targeting vector and a 3′ EGFP-specific antisense primer (P4; 5′-GACACGCTGAACTTGTGGCCGTTTACG) under the following conditions: 15 min of DNA denaturation at 96°C, addition of *Taq* DNA polymerase (Promega, Madison, WI), followed by 94°C for 45 sec and 72°C for 2 min 15 sec (annealing and extension were done at the same temperature) for 38 cycles. Final elongation was done at 72°C for 10 min. PCR was performed using a PTC200 thermocycler (MJ Research, Waltham, MA). The resulting diagnostic amplicon had an estimated size of 2.0 kb (results not shown).

For Southern blot hybridization, DNA of PCR-positive ES cell clones was digested by *Kpn*I and electrophorezed in a 0.7% agarose gel. After blotting of DNA onto Hybond N+ membranes (Amersham Biosciences, Buckinghamshire, UK), the digested DNA was fixed by UV cross-linking. As hybridization probe, we used a labeled external 1 kb *Eco*RV–*Kpn*I fragment (Fig. 1*a*) and a labeled internal 330 bp HPRT-specific *Hind*III–*Xho*I fragment (Güldenagel et al., 2001). Hybridization was performed using Quick Hyb hybridization solution (Stratagene, La Jolla, CA) according to instructions provided by the manufacturer. Final washing was performed under stringent conditions (last wash at 55°C for 15 min in 0.2× SSC and 0.1% SDS). The diagnostic wild type DNA fragment using the external probe had an estimated size of 7.0 kb. Southern blot hybridization using either the external or the internal probe showed a DNA fragment of 12.2 kb containing the targeted Cx47 allele.

Karyotypic analyses, PCR, and Southern hybridization were performed, and positive ES cell clones showing the closest morphological similarity to the original ES cells (Theis et al., 2000) were used for blastocyst injections.

Generation of Cx47^{EGFP} mice

Successfully targeted ES cell clones with an 85–100% diploid karyotype were injected into C57BL/6 blastocysts as described (Theis et al., 2000). After uterus transfer of blastocysts, coat color chimeric mice were born and later crossed with C57BL/6 partners. Offspring mice were checked for germ line transmission by PCR of tail-tip DNA using a Cx47 intron-specific sense primer (P1; 5′-CAGGATCAATGGAAGATTCTCGGTCCC), which was combined with Cx47 exon-specific (P3; 5′-GCCAAGCGGTGGACTGCATAGCCCAGG) and EGFP-specific (P4) antisense primers in a multiplex PCR approach under the following conditions: 5 min of DNA denaturation at 95°C, followed by 40 cycles of 94°C for 45 sec, 64°C for 45 sec, and 72°C for 1 min, and final elongation at 72°C for 10 min. The PCR yielded a 530 bp amplicon specific for wild type and a 340 bp fragment for the mutated Cx47 allele (Fig. 1*c*). Additionally, Southern blot hybridization as described above was used to confirm homologous recombination of the targeting vector (Fig. 1*b*).

Mice heterozygous (+/−) for the Cx47^{EGFP} allele with 50% C57BL/6 genetic background were intercrossed to obtain homozygous Cx47$^{EGFP(-/-)}$ progeny with two EGFP coding alleles under control of the Cx47 promoter and no Cx47 coding DNA, heterozygous Cx47$^{EGFP(+/-)}$ mice with one Cx47 and one EGFP allele, and wild-type Cx47$^{(+/+)}$ littermates that were used for all subsequent studies.

Generation of Cx47/Cx32-double-deficient mice

Cx47$^{EGFP(-/-)}$ male mice were intercrossed with Cx32$^{(-/-)}$ female mice (Nelles et al., 1996), and the F1 generation was intercrossed again to obtain Cx32/Cx47-double-deficient mice. The Cx32 genotype (the Cx32 gene is located on the X chromosome) was tested by tail-tip PCR as described before (Anzini et al., 1997).

Northern blot analysis

Total RNA from different CNS tissues and heart was prepared from Cx47^{EGFP} and wild-type adult mice with the TRIzol reagent (Invitrogen, Karlsruhe, Germany) according to the manufacturer's instructions. The RNA was separated by electrophoresis in a 1% agarose gel and hybridized under stringent conditions as described for Southern blot analysis to a labeled 1.6 kb *Xba*I fragment containing part of the Cx47 coding region and the 3′ untranslated region (Teubner et al., 2001).

Guinea pig polyclonal antibodies to the C terminus of Cx47 (anti-Cx47)

A 16-amino acid peptide (CKGSTGSRDGKATVWI) corresponding to the very end of the cytoplasmic loop of mouse Cx47 was synthesized, coupled, and injected into two Guinea pigs by Eurogentec (Herstal, Belgium). Serum of the final bleeding after the fourth boost was affinity-purified with the same peptide using a HiTrap affinity column (Amersham Biosciences). After elution with 3 M KSCN in PBS and dialysis against PBS, the antibodies were concentrated by Centricon YM-50 centrifugal filter devices (Millipore, Bedford, MA) and finally stored in PBS with 1% BSA and 0.02% sodium azide.

Cx47 immunoprecipitation and Western blot

Western blot analyses of HeLa wild-type, HeLa-Cx47, HeLa-Cx47-EGFP (Teubner et al., 2001), and HeLa-Cx45 (Butterweck et al., 1994) cell lysates with the Cx47 antibodies were prepared. Cultured HeLa cells were harvested and lysed in Laemmli sample buffer as described previously (Traub et al., 1994). After protein quantification, 100 μg of each protein lysate was separated by SDS-PAGE on an 11% gel. Proteins were transferred at 100 V for 120 min in transfer buffer (20 mM Tris, 150 mM glycine, and 20% methanol, pH 8.2) onto Hybond-C extra nitrocellulose (Amersham Biosciences) and blocked for 1 hr in 1× Roti-Block solution (Roth, Karlsruhe, Germany). Incubation with Cx47 antibodies was performed at a 1:1000 dilution in 1× Roti-Block at 4°C overnight. After three washings, the membrane was incubated with ^{125}I-labeled protein A for 3 hr, washed again three times, and exposed to x-ray film overnight.

For immunoprecipitation, freshly prepared tissues [half of the cerebrum, whole cerebellum with brainstem, spinal cord (3 cm), and whole heart] from adult Cx47$^{EGFP(-/-)}$ mice and wild-type Cx47$^{(+/+)}$ littermates were homogenized in 1 ml of ice-cold radioimmunoprecipitation assay (RIPA) lysis buffer [10 mM Na_2HPO_4/NaH_2PO_4, pH 7.2, 40 mM

NaF, 2 mM EDTA, 0.1% SDS, 1% Triton X-100, 0.1% sodium desoxycholate, and 1× Complete protease inhibitor mixture (Roche Molecular Biochemicals, Mannheim, Germany)]. After determination of the protein concentration, the probes were incubated for 3 hr at 4°C with 80 μl of Sepharose Cl-4B (Amersham Biosciences) in TBS and centrifuged (12,000 × *g*, 4°C, 30 min). Affinity-purified Cx47 antibodies (6 μl) were incubated with 20 μl of protein A-Sepharose (Amersham Biosciences) on ice for 2 hr. The precleared lysates were precipitated with the protein A-Sepharose antibody complex overnight at 4°C and washed three times with RIPA wash buffer (10 mM Na_2HPO_4/NaH_2PO_4, pH 7.0, 1 M NaCl, 40 mM NaF, 10 mM EDTA, and 0.2% Triton X-100). The proteins were eluted in 15 μl of Laemmli buffer (65°C, 5 min) and separated by SDS-PAGE on an 11% gel. After protein transfer at 100 V for 75 min in transfer buffer (20 mM Tris, 150 mM glycine, and 20% methanol) onto a Hybond ECL nitrocellulose membrane (Amersham Biosciences), bound proteins were blocked overnight in 1× Roti-Block. To avoid the unwanted detection of the 50 kDa heavy chain of the antibodies used for precipitation, precipitated and blotted Cx47 was detected with Cx47 antibodies that had been biotinylated with NHS-PEO_4-biotin ([15-([biotinoyl]amino)-4,7,10,13-tetraoxapentadecanoic acid, *N*-hydroxysuccinimidylester; Pierce, Rockford, IL]) according to the manufacturer's instructions. They were used at a dilution of 1:500 in 1× Roti-Block for 90 min at room temperature. After three washings (PBS and 0.2% Tween 20), the membrane was incubated (45 min, room temperature, 1:5000) with ImmunoPure Streptavidin (horseradish peroxidase-conjugated; Pierce) and washed again four times. Bound peroxidase was detected using the ECL kit (Amersham Biosciences).

Cx47 immunofluorescence analysis on HeLa cells

To further characterize the Cx47 antibodies, immunolabeling of cultured HeLa-Cx47, HeLa-Cx47-EGFP (expressing a Cx47-EGFP fusion protein; Teubner et al., 2001), and HeLa wild-type cells was performed. HeLa cells, grown on glass coverslips as previously described (Dermietzel et al., 1984), were methanol-fixed for 20 min at −20°C and washed with PBS. To block unspecific binding, the cells were incubated in 4% BSA, 1% goat serum, 0.1% Triton X-100, and 5% low fat milk powder in PBS for 1 hr at room temperature. Cells were then incubated with anti-Cx47 diluted 1:500 in PBS with 4% BSA, 1% goat serum, and 0.1% Triton X-100 at 4°C overnight. After washing, the immunosignals were visualized using 1:3000 diluted Alexa Fluor 594 conjugated goat anti-guinea pig IgG (Molecular Probes, Eugene, OR) in PBS with 4% BSA, 1% goat serum, and 0.1% Triton X-100 and incubated for 2 hr at room temperature. Nuclei of HeLa wild-type and HeLa-Cx47 cells were stained with TOTO-1 (MoBiTec, Goettingen, Germany). After washing with PBS, the coverslips were mounted. For documentation of all fluorescent images, a Zeiss (Jena, Germany) LSM 510 confocal microscope equipped with 2.8 software was used.

Analysis of the EGFP fluorescence reporter signal in mouse nervous tissues

Sixteen-day-old $Cx47^{EGFP}$ mice and wild-type littermates were anesthetized and perfused with 4% paraformaldehyde (PFA) in PBS via the left cardiac ventricle. The brain, spinal cord, optic nerve, and sciatic nerve were isolated, postfixed in 2% PFA in PBS at 4°C overnight, washed in PBS, and incubated in 15% sucrose in PBS for 2 d at 4°C. After embedding in Tissue-Tec (Sakura, Zoeterwoude, The Netherlands), cryostat sections (12 μm) were thawed and mounted on SuperFrost Plus glass slides (Fisher Scientific, Houston, TX), air-dried, and used for immediate fluorescence and immunofluorescence analyses.

For immunofluorescence analyses, the following mouse monoclonal antibodies were applied: (1) to myelin basic protein (MBP) (Serotec, Duesseldorf, Germany), 1:50 diluted; (2) to oligodendrocytic 2′,3′-cyclic nucleotide 3′-phosphodiesterase (CNPase) (Sigma, Saint Louis, MO), 1:500 diluted; (3) to neuronal nuclei (NeuN) (Chemicon, Temecula, CA), 1:400 diluted; and (4) to astrocytic glial fibrillary acidic protein (GFAP; Sigma), 1:500 diluted. Furthermore, rabbit polyclonal antibodies to S100β (Swant, Bellinzona, Switzerland) were used at a dilution of 1:1000. The tissue sections were washed with PBS, and nonspecific binding was blocked by 1% goat serum with 0.1% Triton X-100 in PBS for 20 min at room temperature, followed by 2 hr of blocking in mouse on mouse (MOM) IgG blocking reagent (Vector Laboratories, Burlingame, CA) at room temperature. The primary antibodies were diluted in MOM diluent (Vector Laboratories) and used for incubation at 4°C overnight. Controls were performed without primary antibodies. After two washings in PBS, the specimen were incubated with secondary antibodies (Alexa Fluor 594-conjugated goat anti-mouse; Molecular Probes) diluted 1:400 in MOM diluent or Cy3-conjugated goat anti-rabbit antibodies (Dianova, Hamburg, Germany) diluted 1:1500 for 4 hr at room temperature, washed three times with PBS, mounted on coverslips, and analyzed as described above.

Patch-clamp analysis and single-cell reverse transcription-PCR

Tissue preparation and recording setup. $Cx47^{EGFP(+/-)}$, $Cx47^{EGFP(-/-)}$, and proteolipid protein (PLP)-GFP mice (Fuss et al., 2000) of postnatal ages between 16 and 42 d were used, and frontal brain slices were prepared as described previously (Steinhäuser et al., 1992). For patch-clamp analysis *in situ*, slices were placed in a perfusing chamber installed on the stage of a microscope (Axioskop; Zeiss, Oberkochen, Germany). The chamber was continuously perfused with oxygenated standard solution containing (in mM): 150 NaCl, 5 KCl, 2 $MgSO_4$, 2 $CaCl_2$, 10 HEPES, and 10 glucose, pH 7.4. The pipette solution contained (in mM): 130 KCl, 0.5 $CaCl_2$, 2 $MgCl_2$, 5 1,2-bis(2-amino-phenoxy)ethane-*N,N,N′,N′*-tetraacetic acid, 10 HEPES, and 3 Na_2-ATP, pH 7.2. Recording pipettes were fabricated from borosilicate capillaries (Hilgenberg, Malsfeld, Germany). Recordings (at room temperature) were obtained from GFP-labeled cells located in the stratum oriens of the hippocampal CA1 subregion and the corpus callosum. Membrane currents were measured with the patch-clamp technique in the whole-cell configuration. Signals were amplified (EPC 9/2; HEKA Elektronik, Lambrecht, Germany), filtered (3 or 10 kHz), and monitored with TIDA software (HEKA Elektronik). Capacitance and series resistance compensation (40–50%) were used to improve voltage-clamp control.

Single-cell reverse transcription-PCR. To establish an intron-spanning reverse transcription (RT)-PCR, we screened a rat hippocampus cDNA library (Stratagene 936518). We obtained three independent Cx47 cDNA clones revealing an intron–exon transition at position −28 [position 1 is the first nucleotide of the initiation codon; GenBank (European Molecular Biology Laboratory) accession number AJ276435], a 5112 bp intron, attributable to comparison with mouse genomic DNA, and a 5′ exon of at least 90 bp. Cell harvesting followed a strategy described previously (Schröder et al., 2002). Subsequently, RT was performed in a final volume of ~10 μl, adding an RT buffer (Qiagen, Hilden, Germany), dNTPs (final concentration, 4 × 250 μM; Applied Biosystems, Weiterstadt, Germany), a random hexanucleotide primer (50 μM; Roche Molecular Biochemicals), 20 U of RNasin (Promega), and 0.5 μl of Sensiscript reverse transcriptase (Qiagen). Single-stranded cDNA synthesis was performed at 37°C (1 hr). A nested PCR was performed, using the product obtained after the first round as a template for the second round. The reaction conditions and the purification of the PCR products were similar to those described by Schröder et al. (2002). The Cx47 sense primer was 5′-TAGCCCCACAGTATGCCCTTAG (position −118), and the antisense primer was 5′-CGTCTGCGCTCCTGTTCC (position 308). For the second PCR, the following nested primers were used: sense, 5′-CCGAAGGTTTGCATTTCCAGCCTGGAG (position −57); and antisense, 5′-CAGGTACATGACAGAAGGTGTGG (position 253). Products were identified by agarose gel electrophoresis (1.5%, stained with ethidium bromide) using a molecular weight marker (ΦX174 *Hinc*II digest; Eurogentec, Seraing, Belgium).

For positive control, two-round RT-PCR was performed with 2 ng of DNA-free total mouse RNA and primers as described above. Subsequent gel analysis did not detect any nonspecific products. Amplification of Cx47 in cells of PLP-GFP mice was always paralleled by detection of β-actin as a positive control (Schröder et al., 2002). This approach was not feasible in the case of $Cx47^{EGFP(+/-)}$ mice, presumably because of the decreased amount of Cx47 mRNA attributable to deletion of one allele. Omission of reverse transcriptase served as a negative control and confirmed the specificity of the reaction. The corresponding sense and antisense primers were located on different exons to prevent amplification of genomic DNA. The specificity of RT-PCR was confirmed by

restriction analysis. Thereto, the second PCR round was repeated using 2 μl of the PCR product after the first PCR amplification as a template. The product was purified and dissolved in water (25 μl). The Cx47 cDNA was cut with *Mbo*I (New England Biolabs, Frankfurt, Germany). Seven microliters of the respective PCR product were incubated in 10 U of restriction enzyme (6 hr, 37°C). The cDNA fragments were separated with gel electrophoresis.

Light and electron microscopy of optic nerve and spinal cord

Anesthetized Cx47$^{EGFP(-/-)}$, Cx47$^{EGFP(+/-)}$, and wild-type Cx47$^{(+/+)}$ littermates (5–14 weeks old) as well as Cx32/Cx47-double-deficient mice and their wild-type littermates (4–5 weeks old) were perfused with 6% glutaraldehyde via the left cardiac ventricle. The proximal optic nerve, the intracranial optic nerve, thoracic segments of the spinal cord, and the sciatic nerve were isolated, postfixed in 1% phosphate-buffered OsO_4 in 0.1 M sucrose, and embedded in Epon 812. The semithin sections (1 μm) were stained with toluidine blue and pyronin. Ultrathin sections were contrasted with uranyl acetate as well as lead citrate and examined with a Siemens AG (Erlangen, Germany) electron microscope as described previously (Büssow, 1978).

All animal handling was done in strict accordance with local institutional and governmental guidelines and conformed to the recommendations of the Society for Neuroscience.

Results

Generation of Cx47^{EGFP} mice

We replaced the mouse Cx47 coding region with the EGFP cDNA and the HPRT minigene by homologous recombination (Fig. 1*a*) in HPRT-deficient HM-1 embryonic stem cells (Magin et al., 1992, 1998). Of 232 HAT-resistant clones, 30 clones were screened positive for homologous recombination by PCR. This was verified by Southern blot analysis. Three of these targeted clones were microinjected into C57BL/6 blastocysts (15–20 mutant ES cells per blastocyst). All of these clones yielded high percentages (80–100%) of coat color chimeric mice. At least one male chimeric mouse of each clone led to germ line transmission of the altered Cx47 allele after backcrossing with C57BL/6. Mice with heterozygous deletion of Cx47 [Cx47$^{EGFP(+/-)}$] were intercrossed to obtain Cx47$^{(+/+)}$, Cx47$^{EGFP(+/-)}$, and Cx47$^{EGFP(-/-)}$ littermates. Genotypes were analyzed by PCR (Fig. 1*c*) and Southern blot hybridization (Fig. 1*b*). Cx47^{EGFP} heterozygous (+/−) and homozygous (−/−) mice showed no obvious anatomical or behavioral abnormalities. Female and male Cx47$^{EGFP(-/-)}$ mice were fertile. So far, we have analyzed 14 litters with a total of 106 mice resulting from the interbreeding of Cx47$^{EGFP(+/-)}$ mice. Of these, 22 (21%) were of the Cx47$^{EGFP(-/-)}$ genotype.

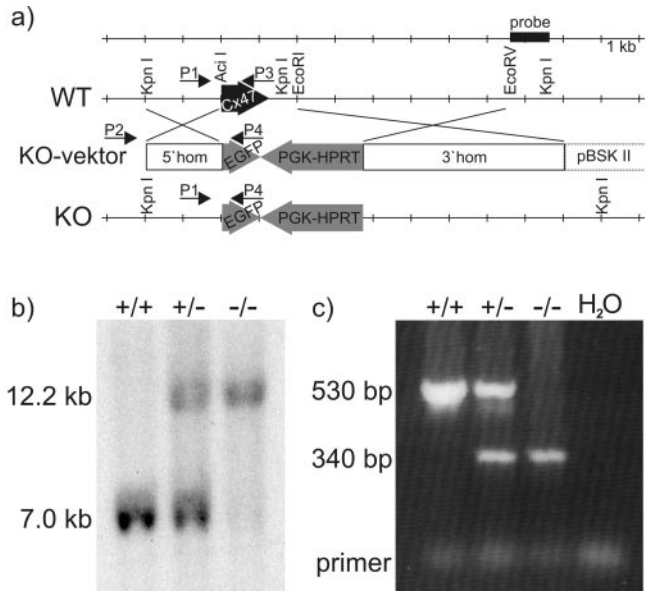

Figure 1. Generation of Cx47-deficient mice with the EGFP reporter gene (Cx47^{EGFP}). *a*, Targeting scheme. WT, Wild-type allele; KO, knock-out allele. The coding region of the wild-type Cx47 gene (black arrow) is located on one exon and includes 1314 bp. After electrotransfecting HM-1 cells with the linearized targeting vector (KO-vektor), homologous recombination occurred in 10% of all clones as determined by PCR using the external sense primer (P2) and the EGFP-specific antisense primer (P4). In the mutated Cx47 allele, the coding region of Cx47 after the first seven codons was replaced by the EGFP cDNA and the PGK-HPRT minigene (gray arrows). The translational start codon of EGFP was cloned in-frame with the Cx47 coding region. The PGK-HPRT minigene was transcribed in the opposite direction. The backbone of the targeting vector consisted of pBlueskript SK II(+) (pBSK II; Stratagene). The 5′ homologous region (5′hom) spanned 2 kb; the 3′ homologous region (3′hom) included 5.5 kb. *b*, Southern blot analysis was performed to confirm homologous recombination. *Kpn*I-digested mouse kidney DNA was probed with a 1 kb external *Eco*RV–*Kpn*I fragment (probe). The 7.0 kb band was derived from the wild-type allele; the larger 12.2 kb band resulted from the knock-out allele. *c*, Diagnostic PCR of tail-tip DNA was performed to screen pedigree mice for occurrence of wild-type and knock-out Cx47^{EGFP} alleles. A multiplex PCR was established using a Cx47 intron-specific sense primer (P1) and a Cx47 exon-specific antisense primer (P3), producing a 530 bp wild-type amplicon and an EGFP-specific antisense primer (P4), resulting in a 340 bp amplicon of the knock-out allele.

The EGFP reporter gene is expressed in accordance with Cx47

The tissue distribution of Cx47 mRNA in mouse has been described previously (Teubner et al., 2001). Cx47 transcripts were mainly detected in brain and spinal cord with an expression peak at approximately day 14 after birth. In addition to this earlier study, Cx47 transcripts were detected by Northern blot analysis in the optic nerve of wild type mice (results not shown). Northern blot analysis of Cx47$^{EGFP(-/-)}$, Cx47$^{EGFP(+/-)}$, and Cx47$^{(+/+)}$ wild-type mice with a probe against Cx47 (Fig. 2*a*) showed the expected decrease of Cx47 mRNA in heterozygous (+/−) and no transcripts in null (−/−) mice. In wild-type (+/+) mice, the strongest expression of Cx47 mRNA was seen in the spinal cord, followed by cerebellum and cerebrum; no signal could be detected in the heart. As expected, EGFP mRNA was found to be expressed instead of Cx47 mRNA and was abundant in homozygous Cx47$^{EGFP(-/-)}$ animals, less frequent in heterozygous animals, and absent in wild-type animals (Fig. 2*b*). The intensity of EGFP mRNA expression in the different tissues tested was proportional to Cx47 mRNA expression in wild-type mice. We conclude that EGFP in these transgenic animals can be considered a reliable replacing reporter for Cx47 transcription.

Characterization of antibodies to Cx47

Antipeptide antibodies to the last 15 amino acid residues of the C-terminal Cx47 region were raised in guinea pigs. This region was selected for immunological reasons; however, it should be noted that it has slight sequence homology with mouse Cx45. Western blot and immunofluorescence analysis were used to characterize the Cx47 antibodies.

Western blot analysis of appropriately transfected HeLa cell lysates with antibodies to Cx47, detected by ^{125}I-labeled protein A, revealed the corresponding Cx47 protein and Cx47-EGFP fusion protein at ~50 and 75 kDa, relative to standard protein markers (Fig. 3*a*). Because EGFP has a molecular mass of 27 kDa, the Cx47-EGFP fusion protein was expected to migrate at ~74 kDa. For HeLa wild-type and HeLa-Cx45 control lysates, no bands could be detected at these positions. Labeled bands with Cx47 antibodies were seen at ~30 and 100 kDa in all HeLa lysates, indicating some cross-reaction of the Cx47 antibodies with other possible proteins.

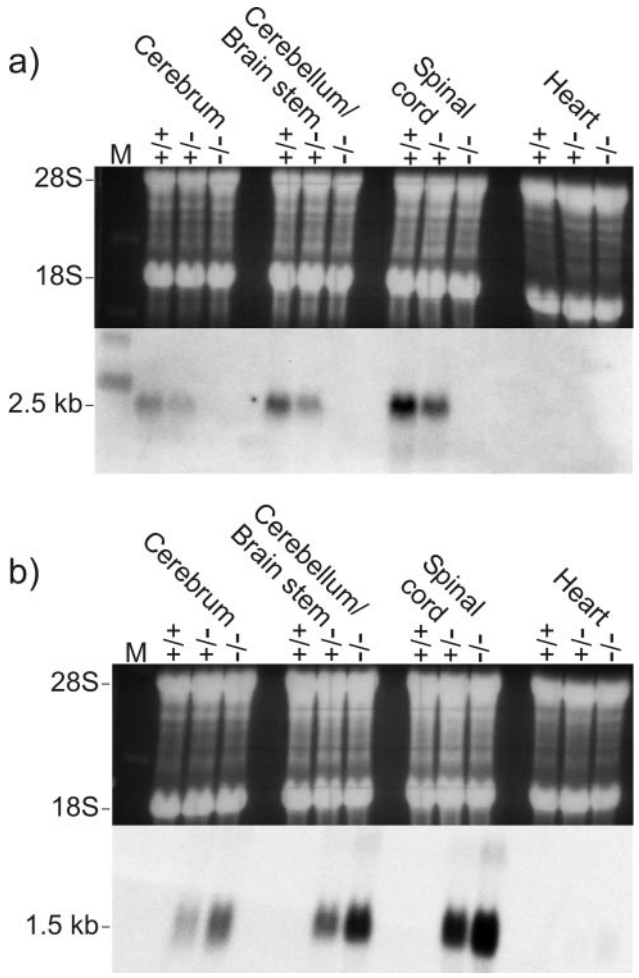

Figure 2. Northern blot analysis of Cx47 expression (*a*) and EGFP expression (*b*) in adult mouse tissues. Equal amounts of total RNA (20 μg) from wild-type (+/+), heterozygous (+/−), and homozygous (−/−) Cx47 ^{EGFP} mice (littermates) were applied as demonstrated by staining of 28S and 18S ribosomal RNA with ethidium bromide (top). The blotted RNA (bottom) was probed with a 1.6 kb *Xba*I fragment containing part of the Cx47 coding region and 3′-untranslated region (*a*) and a 1.0 kb *Sal*I–*Afl*II fragment of the pEGFP-1 vector containing the EGFP-coding region and the SV40 poly(A) signal (b). The size of the corresponding transcripts is indicated in kilobases on the left.

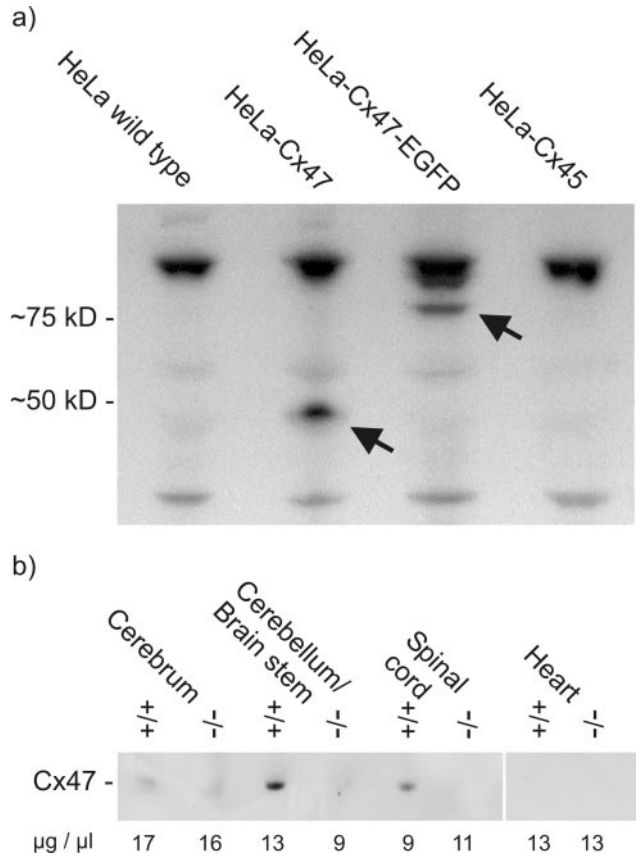

Figure 3. Western blot analysis of protein lysates from different HeLa connexin transfectants (*a*) and after immunoprecipitation of protein lysates from Cx47 wild-type (+/+) and Cx47 $^{EGFP(-/-)}$ mouse tissues (*b*). Western blot analysis with Cx47 antibodies detected by ^{125}I-labeled protein A showed specific bands, at ~50 kDa in HeLa Cx47 lysates and ~75 kDa in HeLa Cx47-EGFP lysates. Nonspecific bands at ~30 and 100 kDa also appeared in control lysates of HeLa wild-type cells and Cx45 transfectants (*a*). Molecular masses are indicated in kilodaltons on the left. By Western blot analysis (ECL) with biotinylated Cx47 antibodies after immunoprecipitation with Cx47 antibodies in lysates of mouse tissue (*b*), Cx47 was found in the cerebellum and spinal cord of wild-type mice; in cerebrum, the signal was very weak. In heart (control tissue) and lysates from Cx47 $^{EGFP(-/-)}$ littermates, no bands were detected. Numbers under each lane represent micrograms of total protein per microliter of lysate of the tissue indicated.

Western blot analyses of mouse tissues using the protocol described above were not successful. Therefore, we used immunoprecipitation to concentrate the Cx47 protein. To avoid interference by the heavy chain of the antibodies used for precipitation, we performed immunodetection with biotinylated Cx47 antibodies using a streptavidin-horseradish peroxidase (ECL) detection system. Under these conditions, the Cx47 protein could be clearly detected in immunoprecipitates of the cerebellum/brainstem and spinal cord of wild-type (+/+) mice (Fig. 3*b*). In immunoprecipitates from Cx47 $^{EGFP(-/-)}$ littermates and in heart control tissue, Cx47 was absent. In cerebrum of wild-type mice, the Cx47 signal was very weak, i.e., only slightly different from the Cx47-null control. The levels of Cx47 protein expression shown in Figure 3*b* cannot be strictly quantitatively compared, because the protein concentrations in lysates prepared from wild-type and Cx47 $^{EGFP(-/-)}$ animals were different, as indicated in Figure 3*b*, and the multiple processing steps involved in immunoprecipitation and subsequent detection might not have been quantitative.

Immunofluorescence analyses with Cx47 antibodies of HeLa cells transfected with Cx47 or Cx47-EGFP showed fluorescent puncta on cell membranes at sites of cell contacts, as expected for gap junction plaques (Fig. 4*a*,*c*). Under the same conditions, immunostaining could be detected neither in HeLa wild-type cells (Fig. 4*b*) nor in HeLa cells stably transfected with Cx45 cDNA (Butterweck et al., 1994) (results not shown). The native EGFP fluorescence of the Cx47-EGFP fusion protein was closely colocalized with the immunofluorescence signals obtained with Cx47 antibodies (Fig. 4*c*,*d*). Cx47 antibodies reacted specifically with Cx47 in HeLa-Cx47 cells. No specific staining was seen after immunofluorescence analysis of mouse wild-type tissue sections in comparison with Cx47-null tissues. Presumably, Cx47 is expressed at a much lower level in mouse CNS than in Cx47-transfected HeLa cells, and the Cx47 antibodies are not sensitive enough to detect low levels of the Cx47 protein.

Localization of EGFP expression in Cx47 ^{EGFP} mice

Analysis of the fluorescent EGFP reporter signal in different nerve tissue sections yielded faint but clear labeling of cell nuclei and perikarya. As expected on the basis of the above results, the EGFP signals were most intense in Cx47 $^{EGFP(-/-)}$ animals at the age of ~2 weeks. The EGFP reporter expression was less intense in older

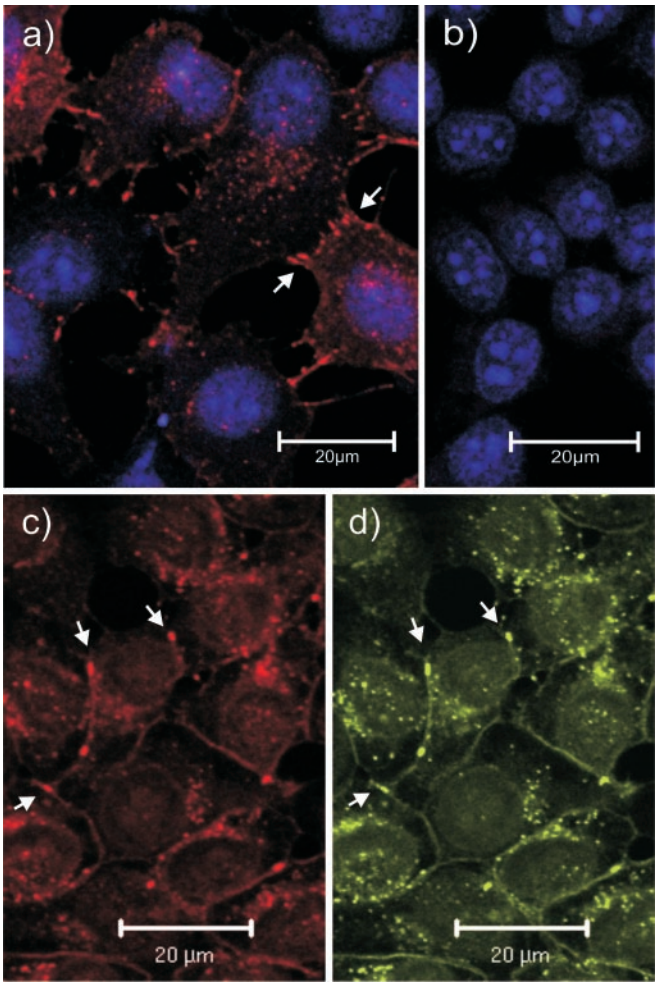

Figure 4. Immunostaining (red) of Cx47 in HeLa-Cx47 (*a*), HeLa wild-type (*b*), and HeLa-Cx47-EGFP (*c*) cells. The EGFP fluorescent signals (*d*, green) corresponding to Cx47-EGFP fusion proteins were primarily colocalized with Cx47 immunofluorescent signals (*c*). Typical punctate gap junction staining was detected on contact membranes of Cx47-transfected cells (arrows), whereas no such staining could be detected in HeLa wild-type controls. Nuclei in HeLa-Cx47 and HeLa wild-type cells were stained with TOTO-1 (blue, false color); nuclei in HeLa-Cx47-EGFP cells were not stained but are visible because of higher background staining. Scale bars, 20 μm.

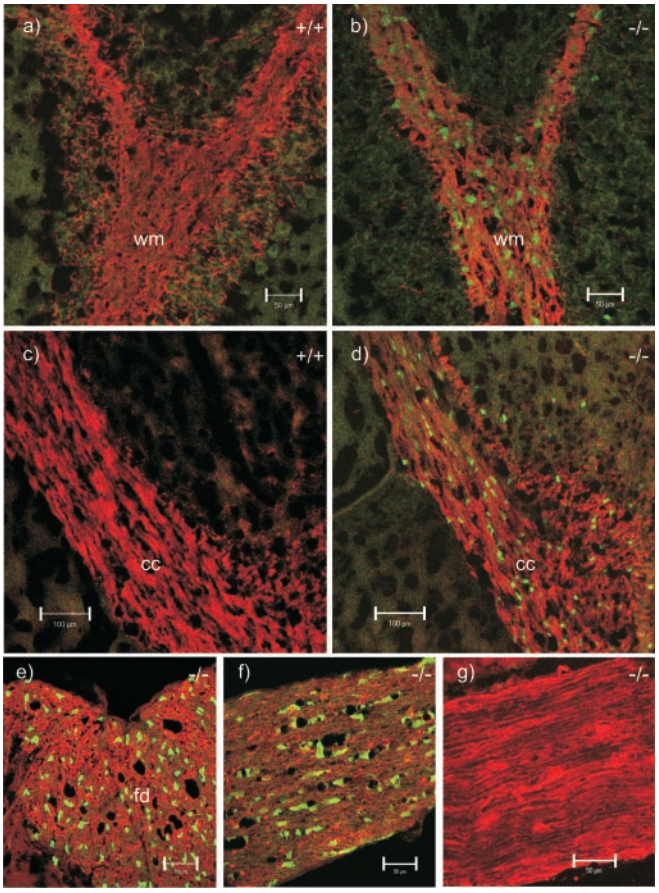

Figure 5. EGFP signal (green) as reporter for Cx47-expressing cells and immunostaining (red) for MBP in wild-type (+/+) and homozygous Cx47^{EGFP} (−/−) mice. Shown are double (red, green) confocal images of cerebellar white matter (wm; *a, b*), corpus callosum (cc; *c, d*), the funiculus dorsalis (fd) in a transverse section of the spinal cord (*e*), a longitudinal section of the optic nerve (*f*), and a longitudinal section of the sciatic nerve (*g*). All corresponding micrographs (*a–g*) were recorded with the same microscope settings. No EGFP signal was observed in wild-type tissues (*a, c*) and Cx47$^{EGFP(-/-)}$ sciatic nerve (*g*). Scale bars: *a, b, e–g*, 50 μm; *c, d*, 100 μm.

and in heterozygous mice. EGFP fluorescence was most frequently but not exclusively detected in cells of the cerebellar white matter (Fig. 5*b*), the corpus callosum (Fig. 5*d*), the spinal cord white matter (Fig. 5*e*), and the optic nerve (Fig. 5*f*). Large numbers of EGFP-labeled cells were also seen in the commissura anterior, the chiasma opticum, and the striatum. No EGFP labeling was found in corresponding wild-type tissues (Fig. 5*a,c*). The sciatic nerve of Cx47$^{EGFP(-/-)}$ animals (Fig. 5*g*), as well as the heart and kidney of these animals (results not shown), were negative for EGFP fluorescence.

Cx47 is expressed in oligodendrocytes and in some S100β-positive cells but not in neurons or in GFAP-positive astrocytes

To further characterize the cellular site(s) of Cx47 expression, immunofluorescence analyses with cell type-specific antibodies in combination with EGFP fluorescence, electrophysiological measurements, and single-cell RT-PCR of EGFP-expressing cells were performed. In the spinal cord, well-characterized neuronal (NeuN) and astrocytic (GFAP) marker proteins showed no colocalizaton with the Cx47 reporter (Fig. 6*b,c*), whereas the oligodendrocytic marker CNPase showed colocalization (yellow) in the cytoplasm close to EGFP-labeled nuclei (Fig. 6*a*). These results were confirmed in several brain regions, including the corpus callosum and cerebellum. Less uniform colocalization was obtained with S100β, a cell marker protein considered astrocyte-specific in gray matter of the CNS (Barger et al., 1992). In particular, colocalization (yellow) of S100β immunostaining and Cx47 EGFP reporter signals was detected in the white matter of spinal cord in heterozygous and homozygous Cx47^{EGFP} mice (Fig. 6*d*). Not all S100β-positive cells expressed the EGFP signal, and not all EGFP-positive cells were positive for S100β. In other brain regions, e.g., the cerebellum, the corpus callosum, or the hippocampus, colocalization between S100β staining and EGFP fluorescence was rarely found. The optic nerve, known to be devoid of neuronal cell bodies, showed strong EGFP labeling with a pearls-on-a-string alignment of labeled cell bodies (Fig. 5*f*), which has previously been described as characteristic for white matter oligodendrocytes (Peters, 1991). No EGFP labeling was detected in the triangular profiles of hippocampal pyramidal cells (CA1–CA4), in granule cells of the dentate gyrus (results not shown), and in the Purkinje cell and granule cell layers of the cerebellum (Fig. 5*b*). These neuronal cells have previously been

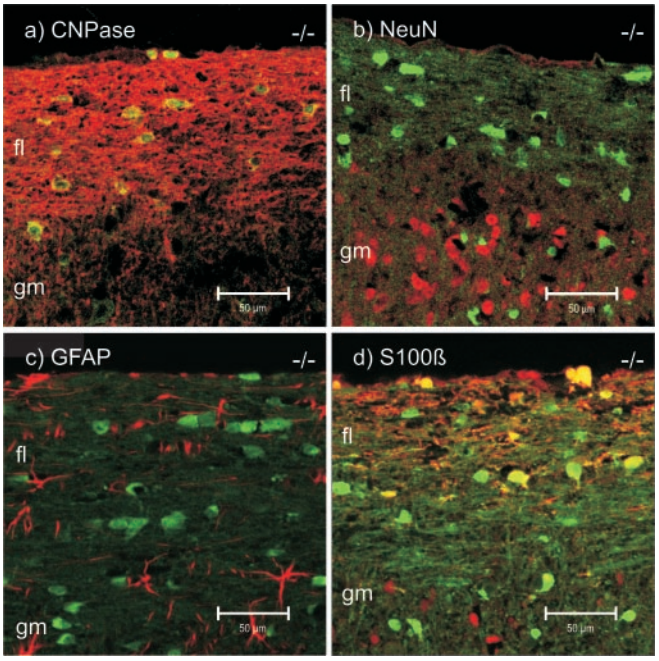

Figure 6. EGFP signal (green) as reporter for Cx47-expressing cells and immunostaining (red) for oligodendrocytic CNPase (*a*), NeuN (*b*), GFAP (*c*), and S100β in longitudinal sections of the spinal cord of Cx47$^{EGFP(-/-)}$ mice. Double (red, green) confocal images are shown. All corresponding images (*a–d*) were recorded with the same microscope settings. CNPase colocalized (yellow) with EGFP fluorescence in the pericaryon (*a*). Cells immunolabeled for NeuN (*b*) were EGFP-negative. Likewise, GFAP-positive cells (*c*) did not express EGFP. A few S100β-positive cells (*d*) expressed EGFP (yellow); others did not (red), but most EGFP-expressing cells were negative for S100β (green). Scale bars, 50 μm. fl, Funiculus lateralis; gm, gray matter.

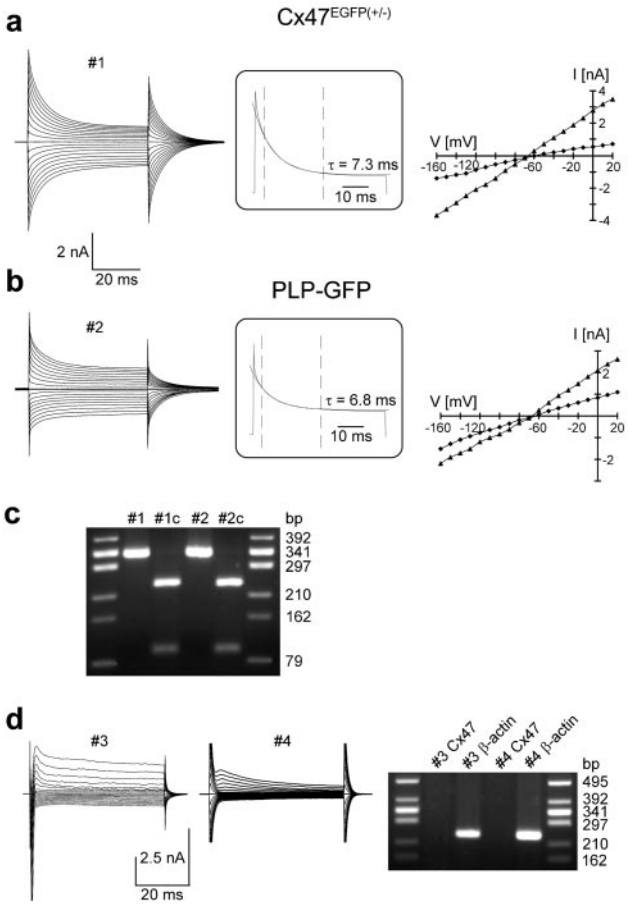

Figure 7. Electrophysiological properties of GFP-labeled cells in Cx47$^{EGFP(+/-)}$ and PLP-GFP mice. Membrane currents were activated between −160 and +20 mV (50 msec; 10 mV increment; holding potential, −70 mV). *a, b*, Right, *I–V* plots when taking amplitudes 2 msec (triangles) and 50 msec (diamonds) after the onset of the voltage steps. *a*, In a fluorescent cell, presumed an oligodendrocyte of the corpus callosum of a Cx47$^{EGFP(+/-)}$ mouse (resting potential, −60 mV), currents reversed at −67 and −59 mV, respectively. *b*, A GFP-positive oligodendrocyte in the corpus callosum of a PLP-GFP mouse (resting potential, −70 mV) displayed reversal potentials of −67 and −64 mV. In both cells, currents decayed with similar time constants as indicated (V, +10 mV; a single exponential was fit to the data recorded between 3 and 25 msec after onset of the voltage steps; time window marked by dashed vertical bars). *c*, Subsequent to functional characterization, the cytoplasm of the cells shown in *a* and *b* was harvested for transcript analysis. PCR products specific to Cx47 (334 bp) were identified by gel electrophoresis (lanes #1, #2 correspond to the cells in *a, b*, respectively). Cx47 cDNA was completely digested by the restriction endonuclease *Mbo*I, yielding fragments of 239 and 95 bp (lanes #1c, #2c). *d*, A GFP-negative CA1 pyramidal neuron (lane #3; PLP-GFP mouse) and an EGFP-negative astrocyte (lane #4; CA1 stratum oriens, Cx47$^{EGFP(+/-)}$ mouse) were analyzed as described above. Both cells lacked Cx47 transcripts, although mRNA of the housekeeping gene β-actin (238 bp) was found (right). As a length marker, *Hinc*II-digested DNA from ΦX174 phages was used.

reported to express Cx47 mRNA on the basis of *in situ* hybridization (Teubner et al., 2001).

Patch-clamp analysis of fluorescent cells in Cx47$^{EGFP(+/-)}$ and PLP-GFP mice

Green fluorescent cells were selected in brain slices from Cx47$^{EGFP(+/-)}$ mice, and membrane currents were evoked between −160 and +20 mV (Fig. 7*a*). Recordings were obtained from cells in the corpus callosum ($n = 16$) and in the stratum oriens of the hippocampal CA1 region ($n = 16$). The protocols activated almost symmetrical outward and inward transmembrane currents, which in most cases (29 of 32 cells) considerably decayed during the voltage steps. Voltage-gated K^+ and Na^+ currents were never observed. The *I–V* relationships were linear or slightly inwardly rectifying, and currents reversed at −66.0 ± 3.9 mV, indicating that they were mainly carried by K^+ (amplitudes taken at the end of the voltage steps; $n = 32$; Fig. 7*a*, right). The current decay could be well fitted by a single exponential yielding time constants of $\tau = 6.3 \pm 2.0$ msec (V, +10 mV; Fig. 7*a*, middle). The resting membrane potential of the cells recorded was −67.4 ± 3.8 mV, and their input resistance, determined from currents evoked by a depolarization from −60 to −50 mV, amounted to 112 ± 66 MΩ.

To compare electrophysiological properties of fluorescent cells in Cx47$^{EGFP(+/-)}$ mice with those of unequivocally identified mature oligodendrocytes, we used transgenic mice with PLP promoter-controlled GFP expression (Fuss et al., 2000). Fluorescent oligodendrocytes were investigated in the corpus callosum ($n = 3$) and in the stratum oriens of the hippocampal CA1 region ($n = 7$) as described above. The whole-cell current patterns evoked upon depolarizing and hyperpolarizing voltage steps (Fig. 7*b*) closely resembled those characteristic of EGFP-positive cells in Cx47$^{EGFP(+/-)}$ mice, with voltage-gated K^+ and Na^+ currents always being absent (Fuss et al., 2000). Resting membrane potential (−65.2 ± 8.9 mV), input resistance (90 ± 55 MΩ), reversal potential of the *I–V* plots (−64.7 ± 7.2 mV), and the kinetics of current decay ($\tau = 6.4 \pm 1.6$ msec, +10 mV; $n = 10$) determined in GFP expressing oligodendrocytes of PLP-GFP mice did not differ from the respective parameters of fluorescent cells in Cx47$^{EGFP(+/-)}$ mice.

Recordings were also obtained from green fluorescent cells in the CA1 stratum oriens and the corpus callosum of Cx47$^{EGFP(-/-)}$ mice ($n = 5$). Resting membrane potential

(−66.6 ± 7.1 mV) and current decay (τ = 6.6 ± 2.2 msec) were similar to the respective parameters determined in cells from PLP-GFP and Cx47$^{EGFP\ (+/-)}$ mice, whereas we noted a somewhat higher input resistance (187 ± 45 MΩ). Tail current analysis was performed to determine the reversal potential (V_{rev}) of the decaying symmetrical currents. Similar to previous reports, V_{rev} was strongly dependent on the duration of the preceding depolarizing test pulse. Prolongation of the test pulse (V, +20 mV) from 1 to 20 msec led to a significant shift in V_{rev} (from −54 ± 12.7 to −18.5 ± 12.6 mV; n = 4), indicating a change in the transmembrane K^+ gradient during the depolarization (results not shown) (cf. Berger et al., 1991; Steinhäuser et al., 1992; Chvatal et al., 1995).

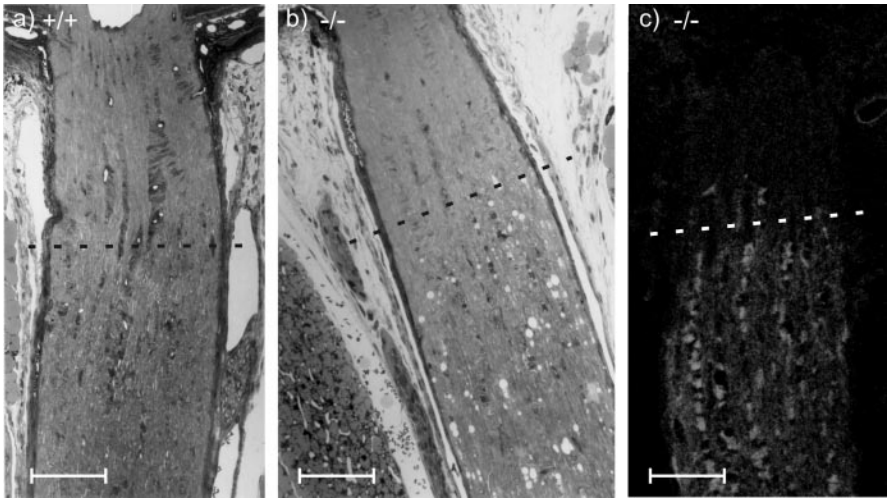

Figure 8. Longitudinal semithin sections of the optic nerve, close to the eye. The partly myelinated transition zone of the optic nerve starts ~250 μm behind the eye bulb (dashed line). In contrast to the wild-type tissue (*a*), the myelinated region of the optic nerve from Cx47$^{EGFP(-/-)}$ mice showed many vacuolated nerve fibers (*b*). Confocal microscopic analysis of EGFP fluorescence (light gray) in the same region of Cx47$^{EGFP(-/-)}$ mice (*c*) demonstrated that Cx47 expression did not occur in front of this transition zone. Scale bars, 100 μm.

Detection of Cx47 transcripts in fluorescent cells of Cx47$^{EGFP(+/-)}$ and PLP-GFP mice

To test for the presence of Cx47 transcripts in green fluorescent cells of both Cx47$^{EGFP(+/-)}$ and PLP-GFP transgenic mice, the cytoplasm of individual cells was harvested subsequent to current analysis, and single-cell RT-PCRs were performed using Cx47-specific primers. Cx47 transcripts were detected in fluorescent cells of Cx47$^{EGFP(+/-)}$ (n = 4) and PLP-GFP (n = 8 of 14) mice. Identity and specificity of the PCR products were confirmed by restriction analysis (Fig. 7*c*). In contrast, no Cx47 transcripts were detected in CA1 pyramidal neurons (n = 4) and in hippocampal astrocytes (n = 4) with different types of voltage-activated K^+ and Na^+ currents (Steinhäuser et al., 1994). The neurons and two of the astrocytes were recorded in PLP-GFP mice; the remaining two astrocytes were from a Cx47$^{EGFP(+/-)}$ mouse (Fig. 7*d*). None of them showed intrinsic fluorescence.

Taken together, our results show that Cx47 is expressed in oligodendrocytes and some S100β-positive cells of the CNS but not in neurons. This corrects our previous incorrect assignment of Cx47 mRNA to certain neurons (Teubner et al., 2001). At that time, Cx47-null mice were not yet generated in our laboratory. Thus, tissues from these mice could not be used as negative controls for *in situ* hybridization.

Cx47-deficient mice display myelination abnormalities

All investigated CNS nerve tissues of homozygous Cx47$^{EGFP(-/-)}$ (n = 4) but not of heterozygous Cx47$^{EGFP(+/-)}$ or wild-type Cx47$^{(+/+)}$ littermates showed sporadic vacuolation of nerve fibers (Figs. 8*b*, 9*b*, 10*a*,*b*). A striking accumulation of these vacuoles was observed in the proximal segment of the optic nerve close to the eye where myelination starts (Hildebrand et al., 1985). Most but not all of the vacuoles were found in internodal regions. There were three different localizations of these vacuoles in relation to the myelin: (1) between the compact myelin and the inner loop (Fig. 10*a*) seen in most of the cases, (2) embedded in compact myelin (Fig. 10*b*), and (3) in direct contact with the periaxonal space (not shown). At all three localizations, the vacuoles were extracellular, surrounded by at least some compact myelin. Similarly vacuolated nerve fibers were reported for myelin under other pathological conditions, for example, in UDP-galactose-ceramide galactosyltransferase-deficient mice (Coetzee et al., 1996; Bosio et al., 1998) and in white matter from sheep with copper poisoning (Ludwin, 1995). Nerve fibers of Cx47$^{EGFP(-/-)}$ animals with no vacuoles showed no obvious difference in myelination compared with Cx47$^{(+/+)}$ wild-type mice. Myelination in the peripheral nervous system of Cx47$^{EGFP(-/-)}$ mice was found to be phenotypically normal.

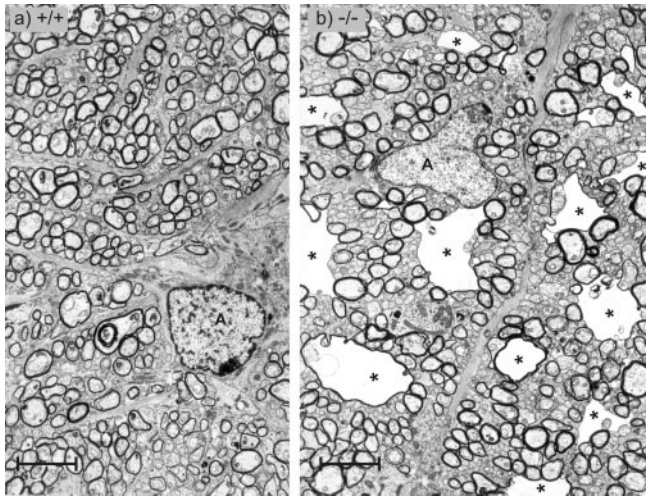

Figure 9. Transverse sections through the partly myelinated transition zone of the optic nerve. In wild-type tissue (*a*) as well as in Cx47$^{EGFP(-/-)}$ tissue (*b*), thin myelin sheets of the first internodes and nonmyelinated nerve fibers were seen. In this transition zone, the vacuolated nerve fibers of the Cx47$^{EGFP(-/-)}$ animal were very prominent (asterisks). *A*, Astrocytes. Scale bars, 3.6 μm.

Cx32/Cx47-double-deficient mice show prominent myelin abnormalities accompanied by a strong action tremor

First analyses of Cx32/Cx47-double deficient mice (Menichella et al., 2001) revealed a phenotype resembling that of the shiverer mouse (cf. Readhead and Hood, 1990), which started 3–4 weeks after birth. These animals died ~3 months after birth.

Preliminary analysis of our Cx32/Cx47-double-deficient mice (n = 9, eight male and one female) showed that these mice de-

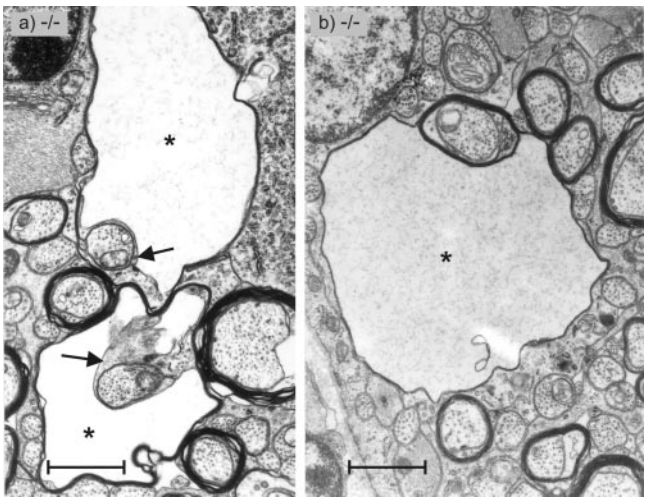

Figure 10. Transverse sections through the partly myelinated transition zone of the optic nerve of Cx47$^{EGFP(-/-)}$ mice as shown in Figure 9. Two types of vacuolated nerve fibers are shown. *a*, The two nerve fibers exhibit vacuoles (asterisks) between the inner lamellae of the oligodendrocyte (arrows) and the compact lamellae of the myelin sheet. *b*, The vacuole (asterisk) of this nerve fiber is located between compact myelin sheets. Scale bars, 1.2 μm.

veloped cumulative neurological abnormalities, starting with a tremor at ~3–4 weeks after birth. Later, they developed tonic seizures and sporadic convulsions. All of them died between 5 and 10 weeks after birth (on average after 51 d). The myelination of the double-deficient mice ($n = 3$ male, 4–5 weeks old) was delayed in development compared with wild-type littermates. Electron microscopy of these double-deficient mice again showed vacuolation as described above for the Cx47$^{EGFP(-/-)}$ mice, which, however, was more severe and more obvious in nerve fibers of all regions of the CNS. Vacuoles were not only predominant in the transition zone of the optic nerve as for the Cx47$^{EGFP(-/-)}$ single-deficient mice but also very prominent at the chiasma opticum (Fig. 11) and in the spinal cord. In contrast to CNS myelin, the peripheral myelin of the Cx32/Cx47-double-deficient mice did not display obvious morphological abnormalities in these 4-week-old mice.

Discussion

In this study, we replaced the Cx47 coding region by EGFP in transgenic mice, which were then used to examine cell type-specific expression and function of Cx47. As expected, deletion of the Cx47 coding region resulted in complete loss of the Cx47 transcript and protein. Homozygous mutant mice developed normally and showed no apparent abnormalities. Northern blot analyses revealed that the EGFP reporter transcript showed a tissue-specific pattern of expression very similar to that of the Cx47 transcript. By single-cell RT-PCR of Cx47$^{EGFP(+/-)}$ mice, we colocalized Cx47 transcript and EGFP expression. In Cx47^{EGFP} mice, EGFP expression was found to be a reliable reporter for Cx47.

Cx47 is expressed in oligodendrocytes

We detected colocalization of EGFP with oligodendrocytic CNPase and found most of the EGFP-labeled cells in highly myelinated, MBP-positive white matter tissue. In contrast, the EGFP (Cx47) reporter signal did not colocalize with neuronal NeuN or astrocytic GFAP cell markers. Together with electrophysiological analysis of EGFP (Cx47)-positive cells, our results show unequivocally that Cx47 is mainly expressed in CNS oligodendrocytes but not in neurons. This has also been reported by Menichella et al. (2001) on the basis of comparative *in situ* hybridizations of wild-type and Cx47 (which was called Cx46.6 by these authors)-deficient mice. Future studies will have to show whether there is a difference between Cx47 expression in white and gray matter oligodendrocytes (Pastor et al., 1998) and whether Cx47 is expressed in all oligodendrocytes or only in some subpopulations. Interestingly, in some cells of spinal cord white matter, the EGFP (Cx47) reporter signal colocalized with S100β. S100β has been described as an astrocytic marker protein in gray matter CNS (Seifert et al., 1997; Savchenko et al., 2000; Kukley et al., 2001). Thus, although S100β expression in spinal cord has not been well characterized, we presume that Cx47 is also expressed by some astrocytes that constitute a strikingly heterogeneous cell population (Matthias et al., 2003).

The assumption of a predominant oligodendroglial location of Cx47 was substantiated by functional and transcriptional analyses of single cells. Patch-clamp recordings revealed that EGFP-positive cells in the corpus callosum and hippocampus of Cx47$^{EGFP(+/-)}$ and Cx47$^{EGFP(-/-)}$ mice showed almost symmetrical, decaying K^+ currents, whereas voltage-gated K^+ or Na^+ currents were never observed. Tail current analyses revealed a significant positive shift in the reversal potential on prolonged membrane depolarization. Cells with a similar whole-cell current profile were previously identified as mature oligodendrocytes in various CNS regions of mouse and rat, and it was suggested that the decaying symmetrical currents reflected a change in the transmembrane K^+ gradient during the voltage steps (Berger et al., 1991; Steinhäuser et al., 1992; Chvatal et al., 1995). The preferential location of Cx47 in CNS oligodendrocytes was further corroborated by the finding that GFP-positive cells in transgenic PLP-GFP mice expressed Cx47 transcripts and displayed transmembrane current patterns similar to those of fluorescent cells in Cx47$^{EGFP(+/-)}$ mice.

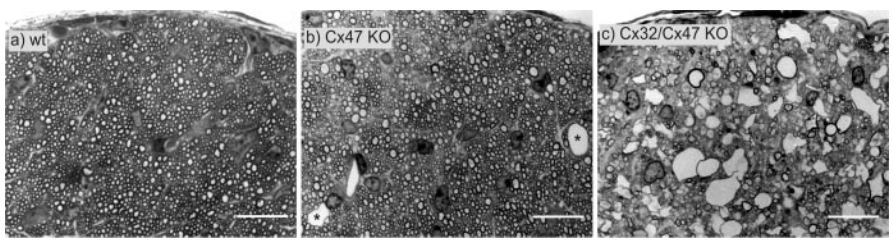

Figure 11. Transverse semithin sections through the intracranial part of the optic nerve immediately in front of the optic chiasm of 4-week-old Cx32$^{(y/+)}$/Cx47$^{(+/+)}$ wild-type (wt; *a*), 5-week-old Cx47$^{EGFP(-/-)}$ single-deficient (*b*), and a Cx32$^{(y/-)}$/Cx47$^{EGFP(-/-)}$ double-deficient (*c*) mice (*b*, *c* are littermates). The double-deficient mice exhibited strongly enhanced vacuolation of nerve fibers all over the CNS, whereas the Cx47$^{EGFP(-/-)}$ mice showed very rare vacuolation (asterisks). Cx47$^{EGFP(-/-)}$ mice exhibited increased vacuolation only in the transition zone of the optic nerve (Fig. 9*b*). KO, Knock-out. Scale bars, 16 μm.

Connexin expression in oligodendrocytes

Together with Cx29 and Cx32, Cx47 is the third connexin described in oligodendrocytes (Dermietzel et al., 1989; Altevogt et al., 2002), indicating some diversity of connexin hemichannels in these cells. In contrast to Cx29 and Cx32, Cx47 is only found in CNS myelinating cells and not in PNS Schwann cells. Previous analyses, which localized Cx45 to oligodendrocytes, were all based on immunohistochemical assays with Cx45 antibodies (Dermietzel et al., 1997; Kunzelmann et al., 1997). We now know that the Cx45 antibodies used

by Kunzelmann et al. (1997) cross-react to some extent with Cx47 protein, which was only identified (Teubner et al., 2001) after the study of Kunzelmann et al. (1997) was published. $Cx45^{+/-}$ mice carrying a lacZ reporter gene (Krüger et al., 2000) do not show β-galactosidase staining in mature oligodendrocytes (Maxeiner et al., 2003).

The present study demonstrates that Cx47 antibodies do not cross-react with Cx45 protein, which exhibits an overall amino acid identity of 49% to Cx47. Although Cx47 protein could easily be detected with Cx47 antibodies in HeLa-Cx47-transfected cells, no specific Cx47 immunofluorescent signals were found in mouse CNS, by comparison with Cx47-deficient tissues. This could be attributable to Cx47-containing gap junction plaques in oligodendrocytes being very small compared with those in HeLa-Cx47 cells. Future analyses, possibly with more sensitive Cx47 antibodies, have to clarify the topological localization of Cx47 protein, which may participate in the formation of gap junctions between oligodendrocytes and neighboring cells (Rash et al., 2001b) or of reflexive gap junctions between different sheets of myelin at paranodal regions of the oligodendrocytes (Sandri et al., 1977; Li et al., 1997).

Redundancy or compensatory regulation of connexin expression in oligodendrocytes may explain the relatively mild phenotype of Cx32-deficient mice (Nelles et al., 1996; Anzini et al., 1997; Scherer et al., 1998) and Cx47-null mice (this work). However, we did not find significant upregulation or downregulation of Cx29 or Cx32 transcripts by Northern blot analysis of $Cx47^{EGFP(-/-)}$ and wild-type tissues (results not shown).

On the other hand, the severe phenotype and the early death of Cx32/Cx47-double-deficient mice point to the functional importance of expressing at least one of these connexins for correct myelination by oligodendrocytes.

Phenotypic abnormalities in Cx47-deficient myelin

The phenotypic abnormality in $Cx47^{EGFP(-/-)}$ mice does not seem to be Cx47-specific but a general indication of disordered myelin (Martini et al., 1998), because similar vacuolation has been reported for other myelin-deficient mice (Bosio et al., 1998) or after copper poisoning of sheep (Ludwin, 1995). In the latter case, vacuoles were explained to indicate the incapability of cells to regulate fluid exchange, which could also arise from disturbed gap junctional intercellular communication. Alternatively, these vacuoles might have developed in response to disturbed signal transduction across myelin or because of a lack of adhesion to other nonconnexin proteins, as proposed for Cx29 (Li et al., 2002), which could result in myelin deformation.

Previously, continuous myelin turnover, irregular myelin, and short internodes have been described to occur in the transition zone of the optic nerve (Hildebrand et al., 1985). The increased appearance of vacuoles in this transition zone of Cx47-deficient mice but not in wild-type littermates suggests that Cx47 may be involved in myelin formation or differentiation of oligodendrocytes. The maximum of Cx47 transcripts at approximately day 14 after birth (Teubner et al., 2001) appears to be in line with this hypothesis. As shown with several other mouse mutants, including Cx32-deficient mice, the immune system appears to be involved in the pathogenesis of some, so far mainly peripheral myelin disorders (Kobsar et al., 2002; Maurer et al., 2002). Therefore, future studies will have to clarify whether microglial cells are also associated with CNS myelin deformation in Cx47-deficient and Cx32/Cx47-double-deficient mice.

References

Altevogt BM, Kleopa KA, Postma FR, Scherer SS, Paul DL (2002) Connexin29 is uniquely distributed within myelinating glial cells of the central and peripheral nervous systems. J Neurosci 22:6458–6470.

Anzini P, Neuberg DH, Schachner M, Nelles E, Willecke K, Zielasek J, Toyka KV, Suter U, Martini R (1997) Structural abnormalities and deficient maintenance of peripheral nerve myelin in mice lacking the gap junction protein connexin 32. J Neurosci 17:4545–4551.

Barger SW, Wolchok SR, Van Eldik LJ (1992) Disulfide-linked S100 beta dimers and signal transduction. Biochim Biophys Acta 1160:105–112.

Berger T, Schnitzer J, Kettenmann H (1991) Developmental changes in the membrane current pattern, K+ buffer capacity, and morphology of glial cells in the corpus callosum slice. J Neurosci 11:3008–3024.

Bosio A, Büssow H, Adam J, Stoffel W (1998) Galactosphingolipids and axono-glial interaction in myelin of the central nervous system. Cell Tissue Res 292:199–210.

Butterweck A, Gergs U, Elfgang C, Willecke K, Traub O (1994) Immunochemical characterization of the gap junction protein connexin45 in mouse kidney and transfected human HeLa cells. J Membr Biol 141:247–256.

Büssow H (1978) Schwann cell myelin ensheathing C. N. S. axons in the nerve fibre layer of the cat retina. J Neurocytol 7:207–214.

Chalfie M, Tu Y, Euskirchen G, Ward WW, Prasher DC (1994) Green fluorescent protein as a marker for gene expression. Science 263:802–805.

Chvatal A, Pastor A, Mauch M, Sykova E, Kettenmann H (1995) Distinct populations of identified glial cells in the developing rat spinal cord slice: ion channel properties and cell morphology. Eur J Neurosci 7:129–142.

Coetzee T, Fujita N, Dupree J, Shi R, Blight A, Suzuki K, Suzuki K, Popko B (1996) Myelination in the absence of galactocerebroside and sulfatide: normal structure with abnormal function and regional instability. Cell 86:209–219.

Cubitt AB, Heim R, Adams SR, Boyd AE, Gross LA, Tsien RY (1995) Understanding, improving and using green fluorescent proteins. Trends Biochem Sci 20:448–455.

Dermietzel R, Leibstein A, Frixen U, Janssen-Timmen U, Traub O, Willecke K (1984) Gap junctions in several tissues share antigenic determinants with liver gap junctions. EMBO J 3:2261–2270.

Dermietzel R, Traub O, Hwang TK, Beyer E, Bennett MV, Spray DC, Willecke K (1989) Differential expression of three gap junction proteins in developing and mature brain tissues. Proc Natl Acad Sci USA 86:10148–10152.

Dermietzel R, Farooq M, Kessler JA, Althaus H, Hertzberg EL, Spray DC (1997) Oligodendrocytes express gap junction proteins connexin32 and connexin45. Glia 20:101–114.

Eiberger J, Degen J, Romualdi A, Deutsch U, Willecke K, Söhl G (2001) Connexin genes in the mouse and human genome. Cell Adhes Commun 8:163–165.

Fuss B, Mallon B, Phan T, Ohlemeyer C, Kirchhoff F, Nishiyama A, Macklin WB (2000) Purification and analysis of in vivo-differentiated oligodendrocytes expressing the green fluorescent protein. Dev Biol 218:259–274.

Güldenagel M, Ammermuller J, Feigenspan A, Teubner B, Degen J, Söhl G, Willecke K, Weiler R (2001) Visual transmission deficits in mice with targeted disruption of the gap junction gene connexin 36. J Neurosci 21:6036–6044.

Hildebrand C, Remahl S, Waxman SG (1985) Axo-glial relations in the retina-optic nerve junction of the adult rat: electron-microscopic observations. J Neurocytol 14:597–617.

Kobsar I, Maurer M, Ott T, Martini R (2002) Macrophage-related demyelination in peripheral nerves of mice deficient in the gap junction protein connexin 32. Neurosci Lett 320:17–20.

Krüger O, Plum A, Kim J-S, Winterhager E, Maxeiner S, Hallas G, Kirchhoff S, Traub O, Lamers WH, Willecke K (2000) Defective vascular development in connexin 45-deficient mice. Development 127:4179–4193.

Kukley M, Barden JA, Steinhäuser C, Jabs R (2001) Distribution of P2X receptors on astrocytes in juvenile rat hippocampus. Glia 36:11–21.

Kunzelmann P, Blumcke I, Traub O, Dermietzel R, Willecke K (1997) Coexpression of connexin45 and -32 in oligodendrocytes of rat brain. J Neurocytol 26:17–22.

Li J, Hertzberg EL, Nagy JI (1997) Connexin32 in oligodendrocytes and association with myelinated fibers in mouse and rat brain. J Comp Neurol 379:571–591.

Li X, Lynn BD, Olson C, Meier C, Davidson KG, Yasumura T, Rash JE, Nagy JI (2002) Connexin29 expression, immunocytochemistry and freeze-

fracture replica immunogold labelling (FRIL) in sciatic nerve. Eur J Neurosci 16:795–806.

Lo CW (1999) Genes, gene knockouts, and mutations in the analysis of gap junctions. Dev Genet 24:1–4.

Ludwin SK (1995) Pathology of the myelin sheath. In: The axon: structure, function and pathophysiology (Waxman SG, Kocsis JD, Stys PK, eds), pp 412–437. New York: Oxford UP.

Magin TM, McWhir J, Melton DW (1992) A new mouse embryonic stem cell line with good germ line contribution and gene targeting frequency. Nucleic Acids Res 20:3795–3796.

Magin TM, Schroder R, Leitgeb S, Wanninger F, Zatloukal K, Grund C, Melton DW (1998) Lessons from keratin 18 knockout mice: formation of novel keratin filaments, secondary loss of keratin 7 and accumulation of liver-specific keratin 8-positive aggregates. J Cell Biol 140:1441–1451.

Martini R, Zielasek J, Toyka KV (1998) Inherited demyelinating neuropathies: from gene to disease. Curr Opin Neurol 11:545–556.

Matthias KF, Kirchhoff F, Seifert G, Hüttmann K, Matyash M, Kettenmann H, Steinhäuser C (2003) Segregated expression of AMPA-type glutamate receptors and glutamate transporters define distinct astrocyte populations in the mouse hippocampus. J Neurosci 23:1750–1758.

Maurer M, Kobsar I, Berghoff M, Schmid CD, Carenini S, Martini R (2002) Role of immune cells in animal models for inherited neuropathies: facts and visions. J Anat 200:405–414.

Maxeiner S, Krüger O, Schilling K, Traub O, Urschel S, Willecke K (2003) Spatiotemporal transcription of connexin45 during brain development results in neuronal expression in adult mice. Neuroscience, in press.

Menichella DM, Sellitto C, Postma FR, Goodenough DA, Paul DL (2001) Normal oligodendrocyte-dependent myelination requires Cx32 and Cx46.6. Paper presented at International Gap Junction Conference, Honolulu, August.

Nelles E, Butzler C, Jung D, Temme A, Gabriel HD, Dahl U, Traub O, Stümpel F, Jungermann K, Zielasek J, Toyka KV, Dermietzel R, Willecke K (1996) Defective propagation of signals generated by sympathetic nerve stimulation in the liver of connexin32-deficient mice. Proc Natl Acad Sci USA 93:9565–9570.

Pastor A, Kremer M, Moller T, Kettenmann H, Dermietzel R (1998) Dye coupling between spinal cord oligodendrocytes: differences in coupling efficiency between gray and white matter. Glia 24:108–120.

Peters A (1991) The neuroglial cells: oligodendrocytes. In: The fine structure of the nervous system, neurons and their supporting cells (Peters A, Palay SL, Webster HD, eds), pp 295–304. New York: Oxford UP.

Rash JE, Yasumura T, Davidson KG, Furman CS, Dudek FE, Nagy JI (2001a) Identification of cells expressing Cx43, Cx30, Cx26, Cx32 and Cx36 in gap junctions of rat brain and spinal cord. Cell Adhes Commun 8:315–320.

Rash JE, Yasumura T, Dudek FE, Nagy JI (2001b) Cell-specific expression of connexins and evidence of restricted gap junctional coupling between glial cells and between neurons. J Neurosci 21:1983–2000.

Readhead C, Hood L (1990) The dysmyelinating mouse mutations shiverer (shi) and myelin deficient (shimld). Behav Genet 20:213–234.

Sandri C, Van Buren JM, Akert K (1977) Membrane morphology of the vertebrate nervous system. A study with freeze-etch technique. Prog Brain Res 46:1–384.

Savchenko VL, McKanna JA, Nikonenko IR, Skibo GG (2000) Microglia and astrocytes in the adult rat brain: comparative immunocytochemical analysis demonstrates the efficacy of lipocortin 1 immunoreactivity. Neuroscience 96:195–203.

Scherer SS, Chance PF (1995) Myelin genes: getting the dosage right. Nat Genet 11:226–228.

Scherer SS, Xu YT, Nelles E, Fischbeck K, Willecke K, Bone LJ (1998) Connexin32-null mice develop demyelinating peripheral neuropathy. Glia 24:8–20.

Schröder W, Seifert G, Huttmann K, Hinterkeuser S, Steinhäuser C (2002) AMPA receptor-mediated modulation of inward rectifier K+ channels in astrocytes of mouse hippocampus. Mol Cell Neurosci 19:447–458.

Seifert G, Zhou M, Steinhäuser C (1997) Analysis of AMPA receptor properties during postnatal development of mouse hippocampal astrocytes. J Neurophysiol 78:2916–2923.

Selfridge J, Pow AM, McWhir J, Magin TM, Melton DW (1992) Gene targeting using a mouse HPRT minigene/HPRT-deficient embryonic stem cell system: inactivation of the mouse ERCC-1 gene. Somat Cell Mol Genet 18:325–336.

Simon AM, Goodenough DA (1998) Diverse functions of vertebrate gap junctions. Trends Cell Biol 8:477–483.

Steinhäuser C, Berger T, Frotscher M, Kettenmann H (1992) Heterogeneity in the membrane current pattern of identified glial cells in the hippocampal slice. Eur J Neurosci 4:472–484.

Steinhäuser C, Kressin K, Kuprijanova E, Weber M, Seifert G (1994) Properties of voltage-activated Na+ and K+ currents in mouse hippocampal glial cells in situ and after acute isolation from tissue slices. Pflügers Arch 428:610–620.

Teubner B, Odermatt B, Güldenagel M, Söhl G, Degen J, Bukauskas F, Kronengold J, Verselis VK, Jung YT, Kozak CA, Schilling K, Willecke K (2001) Functional expression of the new gap junction gene connexin 47 transcribed in mouse brain and spinal cord neurons. J Neurosci 21:1117–1126.

Theis M, Magin TM, Plum A, Willecke K (2000) General or cell type-specific deletion and replacement of connexin-coding DNA in the mouse. Methods 20:205–218.

Traub O, Eckert R, Lichtenberg-Frate H, Elfgang C, Bastide B, Scheidtmann KH, Hülser DF, Willecke K (1994) Immunochemical and electrophysiological characterization of murine connexin40 and -43 in mouse tissues and transfected human cells. Eur J Cell Biol:101–112.

Traub RD, Draguhn A, Whittington MA, Baldeweg T, Bibbig A, Buhl EH, Schmitz D (2002) Axonal gap junctions between principal neurons: a novel source of network oscillations, and perhaps epileptogenesis. Rev Neurosci 13:1–30.

White TW, Paul DL (1999) Genetic diseases and gene knockouts reveal diverse connexin functions. Annu Rev Physiol 61:283–310.

Willecke K, Eiberger J, Degen J, Eckardt D, Romualdi A, Güldenagel M, Deutsch U, Söhl G (2002) Structural and functional diversity of connexin genes in the mouse and human genome. Biol Chem 383:725–737.